Synthesis of Double-Walled Carbon Nanotubes by Catalytic Chemical Vapor Deposition and Their Field Emission Properties

Yang Doo Lee,[†,§] Hyeon Jae Lee,[‡,§] Jong Hun Han,[⊥] Jae Eun Yoo,[⊥] Yun-Hi Lee,[||] Jai Kyeong Kim,[§] Sahn Nahm,[†] and Byeong-Kwon Ju*[,#]

Departments of Materials Science and Engineering, Electronics and Computer Engineering, Physics, and Electrical Engineering, Korea University, Anam-dong, Seongbuk-gu, Seoul 136-713, Republic of Korea, Opto Electronic Materials Research Center, Korea Institute of Science and Technology, 39-1 Hawolgok-dong, Seongbuk-gu, Seoul 136-791, Republic of Korea, and Nanotechnology R & D Center ILJIN Nanotech Co., Ltd., Seoul 157-810, Republic of Korea

Received: August 28, 2005; In Final Form: January 23, 2006

Double-walled carbon nanotubes (DWCNTs) were synthesized by catalytic chemical vapor deposition using Fe−Mo/MgO as a catalyst at 1000 °C under the mixture of methane and hydrogen gas. The nanotubes were purified by acid but were not damaged. Thermogravimetric analysis revealed the purity of the tubes to be about 90%. The high-resolution transmission electron microscopy image showed that DWCNTs have inner tube diameters of 1.4−2.6 nm and outer tube diameters of 2.3−3.4 nm. We observed radial breathing modes in Raman spectra, which are related to the diameter of inner nanotubes. The purified DWCNTs were mixed with organic vehicles and glass frit, and then they were screen-printed on glass substrate coated with indium tin oxide. The field emission properties of the screen-printed DWCNT films were examined by varying the amount of glass frit ingredient within the DWCNT paste. The results showed that DWCNT emitters had good emission properties such as turn-on field of 1.33−1.78 V/μm and high brightness. When the applied anode voltage was gradually increased, current density and brightness became saturated. We also observed DWCNTs adsorbed on the anode plate; they were DWCNTs peeled off from the cathode plate for field emission measurement.

Introduction

Multiwalled carbon nanotubes (MWCNTs)[1] and single-walled carbon nanotubes (SWCNTs)[2,3] have attracted much worldwide attention because of their superb mechanical strength and the unique electronic properties of nanometer scale. Carbon nanotubes (CNTs) are used in applications such as field emission tips,[4] hydrogen storage,[5] transistor,[6] transparent conductive films,[7] and polymer composites.[8] Especially, for field emitters, CNTs have a small diameter and a great aspect ratio as well as high chemical stability and excellent mechanical strength. Field emission display (FED) devices and lighting applications using CNTs as electron emission sources have been fabricated experimentally.[9−11] Basic studies and engineering applications of SWCNTs and MWCNTs have provided great results, but research and applications of double-walled carbon nanotubes (DWCNTs) have been relatively scarce. DWCNTs, consisting of two concentric cylindrical graphene layers, are a type of one-dimensional material between SWCNTs and MWCNTs. The characteristics of DWCNT band structure depend on the combined configuration of the inner and outer tube[12] because of the weak intertube interaction and their stability dependence on the interlayer spacing.[13] Many studies have been carried out on synthesis. Hutchison et al. were the first to produce DWCNTs by arc-discharge technique with catalysts Ni, Co, Fe, and S at 70−80 A in an atmosphere of Ar and H_2 mixture at 350 Torr.[14] Bandow et al. obtained DWCNTs by using C_{60} molecules inside SWCNTs at above 800 °C.[15] Ivanov et al. reported that a small amount of MWCNTs (2−3 walls) of 4 nm diameter was synthesized by catalytic decomposition over a zeolite-supported Co catalyst in N_2–C_2H_2 at 700 °C.[16] Dai et al. obtained SWCNTs with a small amount of DWCNTs by disproportionation of CO at 1200 °C on Al_2O_3-suported Mo catalysts.[17] Recently, DWCNTs have been suggested as field emitters,[18] but field emission properties have been little reported for the DWCNTs so far. In general, vertically aligned CNT emitters can be fabricated by plasma-enhanced chemical vapor deposition[19,20] or by a screen-printing method, which enables us to produce in a large scale.[10, 21]

In this paper, we report on the synthesis of DWCNTs by catalytic chemical vapor deposition of methane (CH_4) with Fe−Mo/MgO catalyst. The structure of DWCNT produced and purified is analyzed by scanning electron microscopy (SEM), high-resolution transmission electron microscopy (HRTEM), Raman spectroscopy, and thermogravimetric analysis. Here, the field emission properties and morphology of screen-printed DWCNT films containing glass frit are also investigated.

Experimental Section

Fe−Mo/MgO catalyst was by the following procedure. A mixture of $Fe(NO_3)_3 \cdot 9H_2O$ (99.99%, Aldrich) and $(NH_4) \cdot 2MoO_4$ (99.98%, Aldrich) was dissolved in ethanol for 1 h. The mixed

[†] Department of Materials Science and Engineering, Korea University.
[§] Opto Electronic Materials Research Center, Korea Institute of Science and Technology.
[‡] Department of Electronics and Computer Engineering, Korea University.
[⊥] Nanotechnology R & D Center ILJIN Nanotech Co., Ltd.
[||] Department of Physics, Korea University.
[#] Department of Electrical Engineering, Korea University.
* Corresponding author. E-mail: bkju@korea.ac.kr. Tel.: +82-2-3290-3237. Fax: +82-2-921-0544.

10.1021/jp0548624 CCC: $33.50
Published on Web 02/24/2006

Fe−Mo solution was then introduced into the suspension of MgO powder in ethanol followed by sonication for 1 h. The average pore diameter and surface area of the MgO powder (Nanoscale Materials Inc.) is 3 nm and 600 m^2/g, respectively. In our experiment, the weight ratio of catalyst was 1:1:40 for Fe/Mo/MgO. After drying, the material was baked in a vacuum oven at 150 °C for 15 h and then ground in a mortar to break the chunks into fine powder. CNTs were synthesized in a quartz tube reactor (20 mm i.d. and 400 mm long) mounted in a tube furnace. Supported Fe−Mo catalyst (200 mg) was placed into a quartz boat at the center of the reactor tube. The quartz tube was heated to 1000 °C in Ar atmosphere. Subsequently, CH_4 (50 sccm) and H_2 (100 sccm) were mixed into the reactor maintained at 1000 °C. After 30 min, the reactor was cooled to room temperature in Ar atmosphere. The crude material was carefully collected from the boat and purified by acid treatment to remove the catalysts. As-grown DWCNTs was immersed in deionized water/hydrochloric acid/nitric acid (4:3:1) mixture and stirred for 30 min, then diluted with deionized water. The obtained suspension was microfiltered with PTFE (polytetrafluoroethylene) membrane filter and rinsed with deionized water. The sample was dried at 130 °C in a vacuum oven for 2 h and then ground in a mortar. The raw and as-purified DWCNTs were characterized by SEM (JEOL JSM-6700F, Hitachi S-4300), HRTEM (JEOL, JEM-3000F, 300 kV), Raman spectroscopy (Jobin Yvon, LabRamHR), and thermogravimetric analysis (TA instrument, TGA Q50). HRTEM analysis was prepared by dispersing a few milligrams of the samples in ethanol in an ultrasonic bath and drying a few drops on a holy-carbon TEM grid. Elemental analysis was carried out on the SEM and HRTEM equipped with an energy-dispersive X-ray spectroscopy (EDS). For Raman measurement, laser excitations were achieved with the 514.5 nm (2.41 eV) line of Ar^+ laser at 2 mW and the 632.8 nm (1.96 eV) line of He−Ne laser at 1.7 mW. Thermogravimetric (TG) analysis was performed on the pure DWCNTs with a ramp rate of 5 °C/min from room temperature to 900 °C at an air flow rate of 100 sccm. The purified DWCNTs were mixed with ethyl cellulose, terpineol, and glass frit. Glass frit ingredient changed 0, 55.5, and 69.0 wt % corresponding to sample A, B, and C, respectively, and DWCNTs were screen-printed on the soda lime glass coated with indium tin oxide (ITO). Cathode plate coated DWCNTs underwent binder burnout at 380 °C in ambient N_2. To activate electron emission, DWCNTs were surface treated by the soft rubbing method. Green phosphor used in the cathode ray tube (CRT) was printed on the ITO glass of the anode plate. The green phosphors were based on ZnS and SiO_2, which were distributed sporadically on the surface of the phosphor particles. Particle size of phosphor and thickness of printed phosphor on ITO glass was 3−4 μm and about 10 μm, respectively. With the gap between anode and cathode of 900 μm, field emissions of DWCNTs were measured in a vacuum chamber at a pressure of 10^{-6} Torr. The sample temperature during the measurement was 300 K. The measured emission area was 1.0 cm^2. Emission current was monitored and controlled by a computer, F.u.g. Elektronix. The brightness, which means here that of cathodoluminescent anode screen, was measured by using a Luminance meter (Topcon Korea Co., BM-902D). Field emission current characteristics of the printed DWCNTs were analyzed.

Results and Discussion

Morphologies and the microscopic structure of purified DWCNTs were examined with SEM, HRTEM, Raman spectroscopy, and TG analysis to evaluate the purification and structural characteristics of the purified DWCNTs. Figure 1a shows a typical SEM image of DWCNTs prepared by using Fe−Mo catalysts supported by MgO. Nodular particles and impurities are present, which are catalyst, support, and carbonaceous particles. This sample was treated with acid to remove catalyst particles, support materials, and impurities. The amount of particles was reduced after purification without any destruction, as can be seen in Figure 1b. Figure 2 shows HRTEM images of the purified DWCNTs. A few black points remaining and still containing amorphous carbon on the tube surface are shown in Figure 2a,b. Elemental analysis showed that metal catalyst remained but Mg was not detected in the purified sample. This result indicates that $HCl-HNO_3$ acid totally dissolved the MgO support, but not the metal catalyst particles because of the presence of their surrounding graphene layers. Long acid treatment caused structural deformation and defects to the nanotubes. Also, dry oxidation damaged the outer wall of the nanotubes, and oxidized metal catalyst particles were not removed.[22] These could be removed only after the complete destruction of nanotubes. Bundles of pure DWCNTs shown in Figure 2a were due to the van der Waals attraction between the tubes. Three-walled CNTs occasionally were found, but the amount was very small and SWCNTs were not observed. In this DWCNTs synthesis, the growth mechanism depended on the metal particles and the support. The outer and inner diameter of the DWCNTs ranged from 2.3 to 3.4 nm and from 1.4 to 2.6 nm, respectively, as shown in Figure 2b. Interlayer spacing of DWCNTs was not constant and ranged from 0.35 to 0.38 nm.

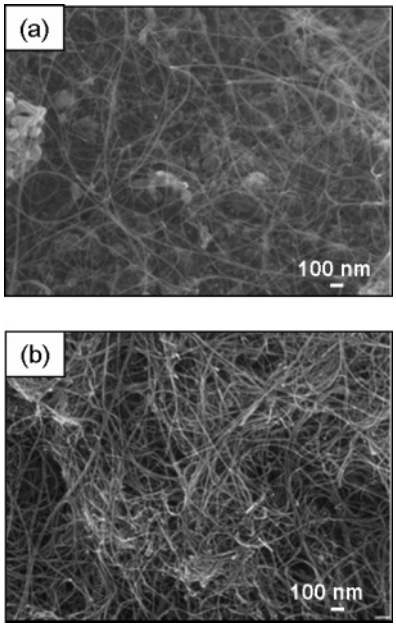

Figure 1. SEM image of synthesized DWCNTs by catalytic decomposition of CH_4 over Fe−Mo/MgO: (a) SEM image of the raw DWCNTs sample and (b) the purified DWCNTs sample by deionized water/HCl/HNO_3 and thermal annealing.

Figure 3 shows the TG analysis result of the purified DWCNTs by acid treatment. TG analysis studies indicated that the purity was 93.7 wt %. The weight reduction of DWCNTs started near 407 °C, and they were completely burnt-off near 600 °C. The remaining materials were transition metals, and the amount was about 6.3 wt %. This curve shows a marked weight loss of about 87% from 498 to 598 °C. The weight starts to decrease sharply from 560 °C, and any amorphous carbon peak from 450 to 500 °C was not observed. This result indicated that most of the amorphous carbon was removed. The acid treatment not only removed most of metal but also produced

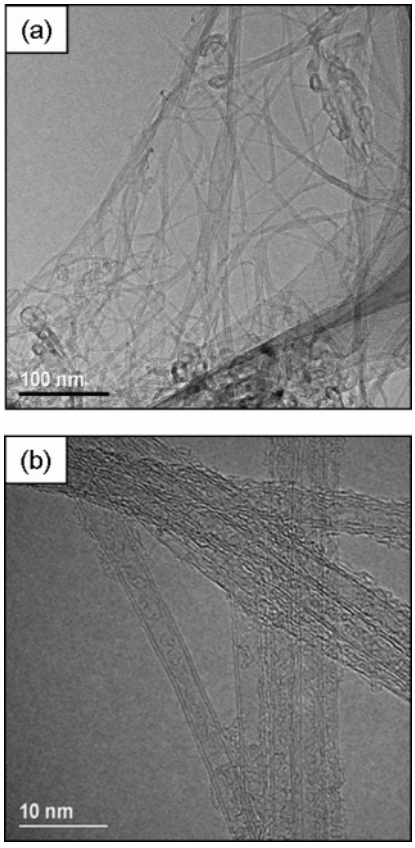

Figure 2. (a) Low-magnification HRTEM image of the purified DWCNTs and (b) that with high magnification.

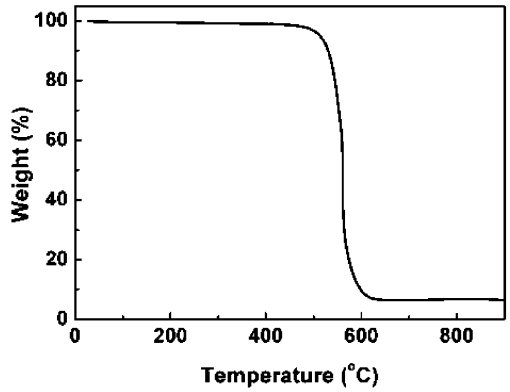

Figure 3. Thermogravimetric analysis of 10 mg samples after acid treatment ramped from 20 to 900 °C at 5 °C per minute under 100 sccm flowing air.

carboxyl, aldehyde, and other functional groups such as −COH, −COOH, etc.[23] on the surface of nanotube. In our purified sample, although a small amount of amorphous carbons still remained, as shown in the Figure 2b, the structure of the nanotube was not destroyed because the nanotube was not treated with oxygen and acid reflux was performed for a short time (30 min).

Raman scattering has become an important tool in the investigation of nanotube properties, such as electronic, phonon, and structural properties.[24,25] The Raman spectra of acid-purified DWCNTs are shown in Figure 4a. In the high-frequency region, the strongest peak G band is located at 1586 cm^{-1}, 1573 cm^{-1} and weak D band is at 1348 cm^{-1}, 1333 cm^{-1} with laser excitation energy (E_{laser}) of 2.41 and 1.96 eV, respectively. The graphite-related tangential G band[26] at 1500−1605 cm^{-1} was derived from Raman-allowed optical mode, which is related to

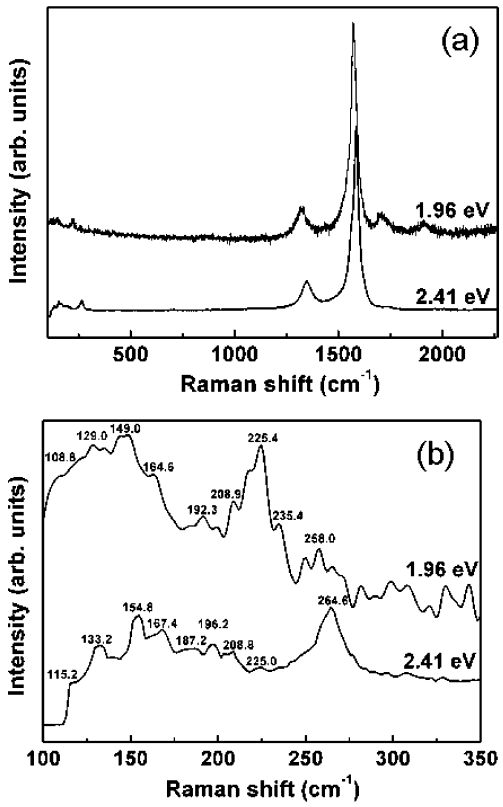

Figure 4. (a) Raman spectrum of purified DWCNTs with laser excitation at 514.5 nm (2.41 eV) and 632.8 nm (1.96 eV). (b) The RBM region in the low-frequency range (100−300 cm^{-1}).

vibration in all sp^2 carbon materials. The disorder-induced D band[26] around 1250−1450 cm^{-1} from the Raman spectra of sp^2-bonded carbon materials is strongly dispersive as a function of E_{laser}. The D band (ω_D) and G band frequencies (ω_G) were changed with different E_{laser}. The peak shifts to higher ω_D and ω_G values with increasing excitation energies.[27−29] Generally, the ratio between the intensity of the G band and D band (I_G/I_D) can be used to show the structural defect and disordered carbon materials in a few micrometers scale. Purified sample shows $I_G/I_D = 4.35$, which was much more than that of raw material: $I_G/I_D = 3.12$ at 2.41 eV. Figure 4b shows the radial breathing mode (RBM) at the low-frequency range from 100 to 300 cm^{-1} with 1.96 and 2.41 eV. Resonance Raman scattering measurements associated with RBM are strongly dependent on the diameters of the tubes.[26,30,31] Due to the influence of the van der Waals interaction in the DWCNT bundles, such as in SWCNT bundles, we used the $\omega_{RBM} = (234/d) + 10$ to calculate the diameter of DWCNT, where ω_{RBM} is the RBM frequency and d is the tube diameter.[30] According to this expression, RBM frequencies in the range of 264.6−115.2 cm^{-1} (with corresponding diameter of 0.92−2.22 nm) and 258.0−108.8 cm^{-1} (with corresponding diameter of 0.94−2.37 nm) are observed in Figure 4b with 2.41 and 1.96 eV, respectively. RBM bands in a lower frequency region are much more difficult to detach due to their large diameter.[28, 31] From these results, the diameter of the tube calculated by RBM is similar to the inner tube diameter value obtained by HRTEM observation. This indicates that the RBMs are related to the inner tube of DWCNTs.[28, 32]

Figure 5a,b shows the field emission curves of the printed DWCNT films and the corresponding Fowler−Nordheim (F−N) plot. Turn-on fields, which correspond to the current density of 1 $\mu A/cm^2$, of samples A, B, and C were measured to 1.39 V/μm, 1.33 V/μm, and 1.78 V/μm, respectively. For each

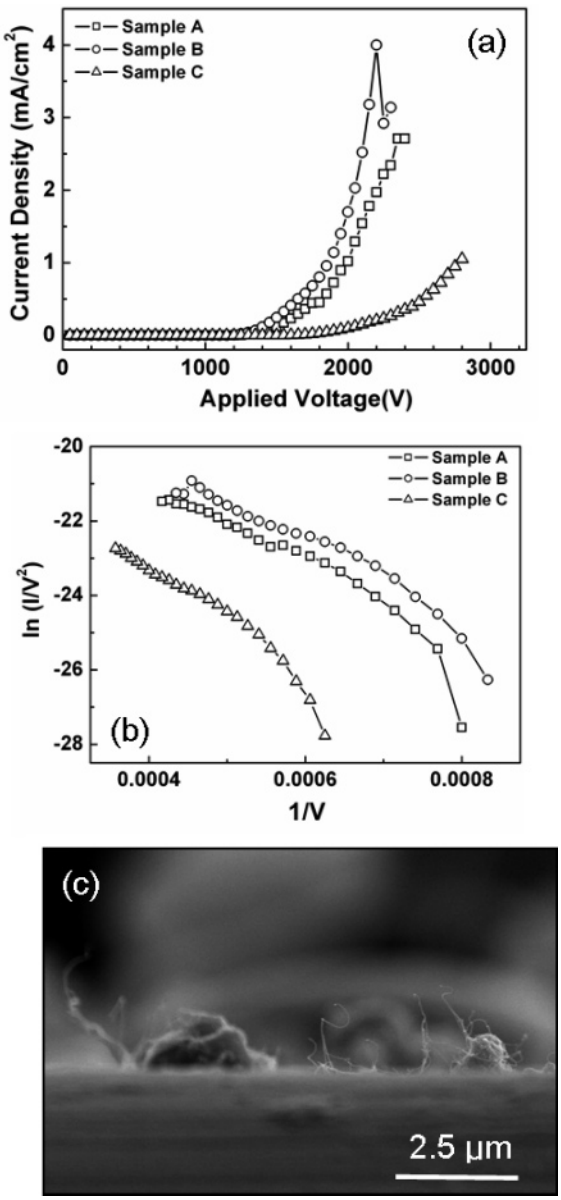

Figure 5. Field emission characteristics of the screen-printed DWCNT cathodes measured in diode mode at 900 μm anode−cathode distance: (a) curves of emission current density versus anode voltage, (b) Fowler−Nordheim plots, and (c) SEM image of printed sample C after field emission.

sample, the emission current density obtained was 1.7 mA/cm^2, 1.02 mA/cm^2, and 0.1 mA/cm^2, respectively, when the anode voltage was 2000 V. It could be explained that the particle governs not only the topography and morphology of the cathode, but also the interface between the particle and matrix.[33] Also, the emission current density was measured as a function of the applied voltage for DWCNT cathodes by using different DWCNTs contents including filler material (glass frit). Printed SWCNT should have a lower turn-on field (1.5−2 V/μm) than that of MWCNT (3 V/μm), and the observation of SWCNT and MWCNT degradation has been reported that the current fluctuations of SWCNTs decreased 20%, while that of MWNTs decreased less than 10%.[34,35] Uemura's work reported that the driving voltage of SWCNTs increased according to the aging time because SWCNTs were fragile; on the other hand, DWCNTs revealed almost no degradation from the constant emission current of 200 μA.[36] SWCNTs have been shown to damage by oxidation (O_2 and H_2O), leading to large fluctuation and degradation. The problem is less serious with MWCNT, and emission current from DWCNT is more stable than that of SWCNT.[37,38] We expect that DWCNT has better emission characteristics than SWCNT and MWCNT. The DWCNT may also have environmental stability better than SWCNT and analogous to MWCNT. Sample A has higher emission current density (4 mA/cm^2 at 2200 V) than samples B and C. At this voltage, brightness was measured to be 40000 cd/m^2, 34300 cd/m^2, and 14730 cd/m^2, whose efficiencies (η, lm/W) were calculated to be 1.2 lm/W, 2.9 lm/W, and 10.1 lm/W, respectively. Efficiency can be expressed as

$$\eta = A/W \text{ lm/m}^2$$

where η denotes the efficiency [lm/W], A is the area [m^2], 1 cd/m^2 = 3.14 lm/m^2, and W is the voltage [V] × the current [A]. The emission area increased with respect to the applied voltage and reached a uniform and total area emission. When the voltage is further increased, anode emission current density and brightness increase, but they become saturated in the range of 2000−2500 V. Because the emission current is charging up in the anode electrode, brightness decreases and the luminous efficiency drops. In the case of sample C, the devices operate stably at high voltage because of the low emission current density, which shows excellent luminous property. To obtain the better efficiency, CRT phosphor needs the high driving voltage. F−N theory[39] is used to describe the field emission behavior of metallic materials applied with high electric field. The theory is expressed by ln(I/V^2) vs 1/V, and is expected to be a straight line. However, the corresponding F−N plots showed distinct nonlinearity in Figure 5b. Especially, the F−N plot of sample C has been fitted by using two straight lines with different slopes. The field emission enhancement factor, β, was calculated from the slopes of F−N plots under the assumption of a work function of 4.5 eV for CNTs, which is a useful parameter for characterizing the field emission properties of CNT arrays. The samples A and B are calculated to be about β = 3775 and 5207, respectively. The β of sample C is 2005 in the low-voltage region, and it increases up to 5030 at high voltage. These results confirm the well-oriented DWCNTs, which induces the main change in the F−N slopes. We believe that the knee occurred by the quantum mechanical tunneling mechanism and aligned DWCNTs. The turn-on fields of the samples are in the order of B < A < C, and emission current density and β are in the order of sample B > A > C, respectively. We cannot clearly explain the difference in the turn-on field, current density, and β. However, the content of DWCNT within the CNT paste and the surface morphology may play a very important role in determining the field emission characteristics. Figure 5c shows SEM image of the printed surface of sample C after field emission. The sample showing an optimal electron emission pattern has the well-aligned DWCNTs in the vertical direction, as shown in Figure 5c. From the field emission measurement, the glass frit strengthens the field emission stability as voltage increases and the vertical arrangement of DWCNT tips.

The original color of phosphors on the anode plate was changed into dark brown color during the field emission measurement. Figure 6 shows an SEM image of DWCNTs adsorbed in the phosphor (the anode plate) after the field emission test in the vacuum chamber. The printed DWCNT emitters where the adhesion is weak fall in the cathode plate and were adsorbed on the anode plate during applied voltage. In addition, a few initial hot emission sites were observed in the low voltage and disappeared when anode voltage was increased. We could observe from the EDS that metal catalysts

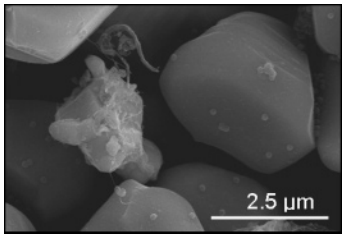

Figure 6. SEM image of DWCNTs adsorbed in the phosphor (the anode plate) after field emission test in a vacuum chamber.

and carbon were detected on the surface of printed phosphors. The anode plate conducted at 500 °C in air for 1 h in a box furnace. DWCNTs attached to phosphors disappeared, and dark varied phosphors returned green color. Therefore, the lifetime of a device is associated with the damaged and broken-away DWCNT from the cathode plate, either directly or indirectly.

Conclusions

To summarize, the structure of synthesized DWCNTs was analyzed, and then the field emission behavior of printed DWCNTs was studied. We prepared DWCNTs by catalytic chemical vapor deposition using Fe−Mo/MgO as catalyst at 1000 °C in CH_4–H_2 gas. DWCNTs were purified by acid treatment to have a purity of 90%. The outer and inner tube diameters of DWCNTs, which were determined from HRTEM images, were in the ranges of 2.3−3.4 nm and 1.4−2.6 nm, respectively. The RBM region of the DWCNTs shows distribution ranging from 0.92 to 2.37 nm. These are similar to inner walls of observed TEM. Purified DWCNTs were mixed with organic vehicles and glass frit. DWCNT cathodes were fabricated by a screen-printing method using DWCNT paste. The field emission properties of screen-printed DWCNTs films were examined by varying the amount of glass frit within the CNT paste. The samples showed DWCNT emitters with good emission properties indicated by a turn-on field of 1.33−1.78 V/μm and high brightness. Sample A without a glass frit has higher emission current density (4 mA/cm^2 at 2200V) than samples B and C, but the efficiency was as low as 1.2 lm/W. However, for samples B and C contained with a glass frit, they have low emission current and higher efficiency than sample A. When the anode voltage was gradually increased, current density and brightness showed values of saturation. If the emission current is greatly increased, the anode plate may break due to thermal shock effect in the applied continuous DC voltage. DWCNTs, the printed emitters on the cathode plate, were adsorbed on the anode plate during field emission measurement due to peeling off the DWCNTs from the cathode.

Acknowledgment. This research has been supported by the Intelligent Microsystem Center (IMC; http://www.microsystem.re.kr), which carries out one of the 21st Century's Frontier R&D Projects sponsored by the Korea Ministry of Commerce, Industry and Energy.

References and Notes

(1) Iijima, S. *Nature* **1991**, *354*, 56.
(2) Bethune, D. S.; Kiang, C. H.; deVries, M. S.; Gorman, G.; Savoy, R.; Vazquez, J.; Beyers, R. *Nature* **1993**, *363*, 605.
(3) Iijima, S.; Ichihashi, T. *Nature* **1993**, *363*, 603.
(4) Rinzler, A. G.; Hafner, J. H.; Nikolaev, P.; Lou, L.; Kim, S. G.; Tománek, D.; Nordlander, P.; Colbert, D. T.; Smalley, R. E. *Science* **1995**, *269*, 1550.
(5) Dillon, A. C.; Jones, K. M.; Bekkendahl, T, A.; Kiang, C. H.; Bethune, D. S.; Heben, M. J. *Nature* **1997**, *386*, 377.
(6) Tans, S. J.; Devoret, M. H.; Dai, H.; Thess, A.; Smalley, R. E.; Geerligs, L. J.; Dekker: C. *Nature* **1997**, *386*, 474.
(7) Wu, Z.; Chen, Z.; Du, X.; Logan, J. M.; Sippel, J.; Nikolou, M. Kamaras, K.; Reynolds, J. R.; Tanner, D. B.; Hebard A. F.; Rinzler, A. G. *Science* **2004**, *305*, 1273.
(8) Olek, M.; Ostrander, J.; Jurga, S.; Mohwald, H.; Kotov, N.; Kempa, K.; Giersig, M. *Nano Lett.* **2004**, *4*, 1889.
(9) Wang, Q. H.; Setlur, A. A.; Lauerhaas, J. M.; Dai, J. Y.; Seelig, E. W.; Chang, R. H. *Appl. Phys.* Lett. **1998**, *72*, 2912.
(10) Choi, W. B.; Chung, D. S.; Kang, J. H.; Kim, H. Y.; Jin, Y. W.; Han, I. T.; Lee Y. H.; Jung, J. E.; Lee, N. S.; Park, G. S.; Kim, J. M. *Appl. Phys. Lett.* **1999**, *75*, 3129.
(11) Saito, Y.; Uemura, S.; Hamaguchi, K. *Jpn. J. Appl. Phys.* **1998**, *37*, L346.
(12) Tanaka, K.; Aoki, H.; Ago, H.; Yamabe, T.; Okahara, K. *Carbon* **1997**, *35*, 121.
(13) Saito, R.; Matsuo, R.; Kimura, T.; Dresselhaus, G.; Dresselhaus, M. S. *Chem. Phys. Lett.* **2001**, *348*, 187.
(14) Hutchison, J. L.; Kiselev, N. A.; Krinichnaya, E. P.; Krestinin, A. V.; Loutfy, R. O.; Morawsky, A. P.; Muradyan, V. E.; Obraztsova, E. D.; Sloan, J.; Terekhov, S. V.; Zakharov, D. N. *Carbon* **2001**, *39*, 761.
(15) Bandow, S.; Takizawa, M.; Hirahara, K.; Yudasaka, M.; Iijima, S. *Chem. Phys. Lett.* **2001**, *337*, 48.
(16) Ivanov, V.; Fonseca, A.; Nagy, J. B.; Lucas, A.; Lambin, P.; Bernaerts, D.; Zhang, X. B. *Carbon* **1995**, *33*, 1727.
(17) Dai, H.; Rinzler, A. G.; Nikolaev, P.; Thess, A.; Colbert, D. T.; Smalley, R. E. *Chem. Phys. Lett.* **1996**, *260*, 471.
(18) Uemura, S.; Yotani, J.; Nagasako, T.; Kurachi, H.; Yamada, H.; Ezaki, T.; Maesoba, T.; Nakaoet, T.; Saito, Y.; Yumura, M. *SID Symposium Digest of Technical Papers*, **2002**, 1132.
(19) Fan, S.; Chapline, M. G.; Franklin, N. R.; Tombler, T. W.; Cassell, A. M.; Dai, H. *Science* **1999**, *283*, 512.
(20) Ren, Z. F.; Huang, Z. P.; Xu, J. W.; Wang, J. H.; Bush, P.; Siegal, M. P.; Provencio, P. N. *Science* **1998**, *282*, 1105.
(21) Kim, Y. C.; Sohn, K. H.; Cho, Y. M.; Yoo, E. H. *Appl. Phys. Lett.* **1999**, *84*, 5350.
(22) Biróa, L. P.; Khanha, N. Q.; Vértesya, Z.; Horvátha, Z. E.; Osvátha, Z.; Koósa, A.; Gyulaia, J.; Kocsonyab, A.; Kónyac, Z.; Zhangd, X. B.; Van Tendelood, G.; Fonsecae, A.; Nagye, J. B. *Mater. Sci. Eng. C* **2002**, *19*, 9.
(23) Kinoshita, K. *Carbon: Electrochemical and Physicochemical Properties*; Wiley: New York, 1988; Chapter 3.
(24) Rao, A. M.; Richter, E.; Bandow, S.; Chase, B.; Eklund, P. C.; Williams, K. A.; Fang, S.; Subbaswamy, K. R.; Menon, M.; Thess, A.; Smalley, R. E.; Dresselhaus, G.; Dresselhaus, M. S. *Science* **1997**, *275*, 187.
(25) Richter, E.; Subbaswamy, K. R. *Phys. Rev. Lett.* **1997**, *79*, 2738.
(26) Dresselhaus, M. S.; Dresselhaus, G.; Jorio, A.; Souza Filho, A. G.; Saito, R. *Carbon* **2002**, *40*, 2043.
(27) Brown, S. D. M.; Jorio, A.; Dresselhaus, M. S.; Dresselhaus, G. *Phys. Rev. B* **2001**, *64*, 073403.
(28) Kim, D. Y.; Yang, C. M.; Park, Y. S.; Kim, K. K.; Jeong, S. T.; Han, J. H.; Lee, Y. H. *Chem. Phys. Lett.* **2005**, *413*, 135.
(29) Sangaletti, L.; Pagliara, S.; Parmigiani, F.; Galinetto, P.; Larciprete, R.; Lizzit, S.; Goldoni, A. *Eur. Phys. J. B* **2003**, *31*, 203.
(30) Kuzmany, H.; Plank, W.; Hulman, M.; Kramberger, Ch.; Grüneis, A.; Pichler, Th.; Peterlik, H.; Kataura, H.; Achiba, Y. *Eur. Phys. J. B* **2001**, *22*, 307.
(31) Hutchison, J. L.; Kiselev, N. A.; Krinichnaya, E. P.; Krestinin, A. V.; Loutfy, R. O.; Morawsky, A. P.; Muradyan, V. E.; Obraztsova, E. D.; Sloan, J.; Terekhov, S. V.; Zakharov, D. N. *Carbon* **2001**, *39*, 761.
(32) Qiu, H.; Shi, Z.; Guan, L.; You, L.; Gao, M.; Zhang, S.; Qiu, J.; Gu, Z. *Carbon* **2006**, *44*, 516.
(33) Burden, A. P.; Bishop, H. E.; Brierley, M.; Friday J. M.; Hood, C.; Jones, P. G. A.; Khazov, A. Y.; Lee, W.; Riggs, R. J.; Shaw, V. L.; Tuck, R. A. *J. Vac. Sci. Technol. B* **2000**, *18*, 900.
(34) Kim, K.-B.; Song, Y.-H.; Hwang, C.-S.; Chung, C.-H.; Lee, J.-H.; Choi, I.-S.; Park, J.-H. *J. Vac. Sci. Technol. B* **2004**, *22*, 1331.
(35) Chung, D. S.; Choi, W. B.; Kang, J. H.; Kim, H. Y.; Han, I. T.; Park, Y. S.; Lee, Y. H.; Lee, N. S.; Jung, J. E.; Kim, J. M. *J. Vac. Sci. Technol. B* **2000**, *18*, 1054.
(36) Uemura, S.; Yotani, J.; Nagasako, T.; Kurachi, H.; Yamada, H.; Ezaki, T.; Maesoba, T.; Nakao, T. *SID '02*; The Society for Information Display: Boston, 2002; p 1132.
(37) Kenneth, A. D.; Chalamala, B. R. *Appl. Phys. Lett.* **1999**, *75*, 3017.
(38) Son, Y. W.; Oh, S.; Ihm, J.; Han, S. *Nanotechnology* **2005**, *16*, 125.
(39) Spindt, C. A.; Brodie, I.; Humphrey, L.; Westerberg, E. R. *J. Appl. Phys.* **1976**, *47*, 5248.